Pflügers Arch – Eur J Physiol (1998) 436:497–508

ORIGINAL ARTICLE

Soh Hidaka · Andrew T. Ishida

Voltage-gated Na^+ current availability after step- and spike-shaped conditioning depolarizations of retinal ganglion cells

Received: 9 October 1997 / Received after revision: 30 March 1998 / Accepted: 15 April 1998

Abstract We used two conditioning voltage protocols to assess inactivation of voltage-gated Na^+ current in retinal ganglion cells. The first protocol tested the possibility, raised by published activation and steady-state inactivation curves, that Na^+ ions carry a "window" current in these cells. The second protocol was used, because these cells spike repetitively in situ, to measure the Na^+ current available for activation following spikes. Na^+ current activated at test potentials more positive than –65 mV. At test potentials more positive than –55 mV, Na^+ current peaked and then declined along a time course that could be fit by the sum of a large, rapidly decaying component, a small, slowly decaying component and a non-decaying component. Both step- and spike-shaped conditioning depolarizations reduced the amount of current available for subsequent activation, sparing the non-decaying "persistent" component. Most of the Na^+ current recovered from this inactivation along a rapid exponential time course (τ=3 ms). The remaining recovery was complete within at least 4 s (at –70 mV). Our use of step depolarizations has identified a current component not anticipated from previous measurements of steady-state inactivation in retinal ganglion cells. Our use of spike-shaped depolarizations shows that Na^+ current density at 1 ms after a single spike is roughly 25% of that activated by the conditioning spike, and that recovery from inactivation is 50–90% complete within 10 ms thereafter. Na^+ current amplitude declines during spikes repeated at relatively low frequencies, consistent with a slow component of full recovery from inactivation.

Key words Excitability · Partial inactivation · Persistent Na^+ current · Retinal ganglion cell · Sub-threshold current

S. Hidaka · A.T. Ishida (✉)
Section of Neurobiology, Physiology, and Behavior,
University of California, One Shields Avenue,
Davis, CA 95616–8519, USA

Introduction

The ability of neurons to produce trains of action potentials requires that a net inward current can be activated momentarily and repeatedly. Although this current is carried in many cells by Na^+ ions, spikes depolarize cells to membrane potentials that increase inactivation of voltage-gated Na^+ current [27]. The capacity to spike repetitively can be guarded by various means. Delayed outward currents commonly hasten repolarization between spikes to membrane potentials that relieve Na^+ current, at least partially, from inactivation. Amounts of Na^+ current available for repetitive spiking could also be enhanced. For example, Na^+ current that inactivates completely at depolarized membrane potentials could be increased around threshold by adjusting the overlap of activation and steady-state inactivation curves [3, 16]. A different means of augmenting Na^+ current would be to reduce its susceptibility to steady-state inactivation. Na^+ currents that are activated, but not altogether inactivated, by depolarization were first recognized in axons [8, 12, 18, 23] and subsequently found in neuronal somata [37, 48, 49], dendrites [29, 39, 46], cardiac muscle [40, 44], skeletal muscle [11, 41], and neuroblastoma cells [42].

Particularly in sensory systems, stimulus properties that trigger and modulate repetitive spiking have been studied more widely than its mechanisms. Because they encode easily controlled and behaviorally important stimuli, retinal ganglion cells have long been prime subjects of these and related investigations (see [43]). However, several properties of the voltage-gated ion conductances that enable these cells to spike repetitively and at different frequencies are not fully understood. More than a dozen conductances have recently been identified in voltage-clamped retinal ganglion cells [31], and two pertinent properties of Na^+ currents have been measured. First, Na^+ current activation threshold has generally been found to be around –45 mV, although reported values range from –50 to –31 mV [5, 30, 33]. Secondly, Na^+ currents have been found to inactivate completely around –20 mV [5, 35, 38]. Because these results suggest that retinal ganglion cells

can generate a "window" type of Na^+ current [3], we have measured Na^+ currents that are activated and inactivated by step-wise depolarizations. Because retinal ganglion cells can spike repetitively without repolarizing to the resting potential or more negative membrane potentials between spikes, we have also measured the Na^+ current that is inactivated by depolarizations shaped like spikes recorded from these cells under current clamp. Some of these results have appeared in a meeting abstract [25].

Materials and methods

The action potentials and voltage-clamp currents described below were measured from single, neurite-free retinal ganglion cell somata isolated from common goldfish (*Carassius auratus*; 9–16 cm body length). Recordings were made from these somata in vitro for four reasons: (1) to minimize persistent current attributable to inhomogeneous space clamp [56]; (2) to facilitate both the control of cytoplasmic Na^+ ion concentrations and the reduction of contaminating outward currents [30, 31]; (3) to test predictions based on previous measurements of somatic Na^+ current voltage-sensitivity (see Introduction); and (4) because fish retinal ganglion cell somata display Na^+ channel-like immunoreactivity in situ (Yoshikawa, Sakaguchi, Anderson, Flannery, FitzGerald, and Ishida; unpublished results). Retinal dissociation, cell identification, bath superfusion with control solution, application of test solutions by microperfusion, and liquid junction potential correction were performed as described elsewhere [9, 30, 51]. Whole-cell patch-clamp recordings were performed in either perforated-patch or ruptured-patch mode [45], using a standard amplifier (L/M-EPC 7, List Electronic, Darmstadt Germany; or Axopatch-1D, Axon Instruments, Foster City, Calif., USA) at room temperature (approx. 23°C) within 10 h of each retinal dissociation. The voltage dependence of steady-state inactivation was stable for 20–60 min in perforated-patch mode, whereas the voltage of 50% steady-state inactivation ($V_{1/2}$) (see Results) drifted negatively by 10–20 mV after around 10 min in ruptured-patch mode. Before this drift developed, similar values of activation threshold, decay kinetics, and steady-state inactivation were obtained with these two recording methods, and are therefore pooled in the Results. Recovery from inactivation was measured only in perforated-patch mode.

Patch electrodes were pulled from borosilicate glass capillaries to tip resistances of 2.5–3.5 MΩ. Ruptured-patch pipette solution consisted of (in mM): 110 tris(hydroxymethyl) aminomethane (or 100 CsOH plus 10 CsCl), 4 NaCl, 30 tetraethylammonium chloride (TEA-Cl), 10 1,2-bis(2-aminophenoxy)ethane-*N*,*N*,*N*',*N*'-tetraacetic acid (BAPTA), 0.5 $CaCl_2$, 2 $MgCl_2$, 5 Mg-ATP, 0.8 Na_2GTP, 10 HEPES. The pH of this solution was adjusted to 7.5 with methanesulfonic acid (MSA), and osmolality was adjusted to 310–320 mosmol/kg with sucrose. TEA^+ and Cs^+ were included in this solution to block outward K^+ currents. The calculated free Ca^{2+} concentration was approximately 3 nM. Transient and persistent Na^+ currents similar to those described here were also recorded with pipette solutions containing free Ca^{2+} levels calculated to be 100 nM, and total Cl^- levels of 150 mM.

Perforated-patch pipette tips were filled with (in mM): 110 CsOH, 30 TEA-Cl, 4 NaCl, 0.5 $CaCl_2$, 2 $MgCl_2$, 10 BAPTA, 10 HEPES; pH and osmolality were adjusted to 7.5 with MSA, and 300–310 mosmol/kg with sucrose, respectively. The shank of these pipettes was filled with this solution after addition at 1:125 of a solution containing 2 mg Amphotericin B (Sigma; St. Louis, Mo., USA) plus 3 mg Pluronic F-127 (Molecular Probes; Eugene, Ore., USA) in 60 µl DMSO (Sigma). Perforation was achieved within 4–30 min after cell-attached mode formation.

Control external ("bath") solution consisted of (in mM): 110 NaCl, 5 CsCl, 30 TEA-Cl, 3 4-aminopyridine, 0.1 or 0.3 $CaCl_2$, 2.4 $CoCl_2$, 10 D-glucose, and 10 HEPES; pH and osmolality were adjusted to 7.5 with CsOH, and 320–330 mosmol/kg with sucrose, respectively. Co^{2+}, TEA^+, 4-aminopyridine, and Cs^+ were included in this solution to block voltage-gated Ca^{2+}, K^+, and mixed-cation (I_h) currents, respectively [9, 30, 51]. To facilitate measurement of the persistent Na^+ current in some experiments, bath Na^+ was increased to 150 mM (by adding 40 mM NaCl to the above solution, while reducing TEA to 10 mM). Test solutions were made by addition of TTX to control bath solution, by equimolar substitution of LiCl for NaCl, or by either partial or total isosmotic substitution of NMG-HCl for NaCl (e.g., in Figs. 2 and 3). TTX (no. 584411, Calbiochem-Novabiochem; La Jolla, Calif., USA) was dissolved in water to a stock concentration of 1 mM, and diluted in control bath solution to the concentrations used. Mean Na^+ current amplitudes under various conditions are pooled from the indicated numbers of cells, and reported together with ±1 SEM. Each Na^+ current density reported here (in pA/pF) was calculated by dividing current amplitude (at the peak or non-decaying phase) by the membrane capacitance of the cell from which the recording was made (as gauged by capacitive current cancellation; range: 13–35 pF).

Voltage protocols, P/4 linear leak subtraction (when command voltage changes were all step-wise), and off-line analysis were performed with the pCLAMP system (v. 6.0.2, Axon Instruments). The current monitor output of the patch-clamp amplifier was analog-filtered with a Bessel filter [either that built-in to the Axopatch 1D, or Model 902 (Frequency Devices; Haverhill, Mass., USA) in series with the List EPC-7; corner frequency=1 or 2 kHz] and digitally sampled at twice the filter frequency (or faster). Na^+ current decay was fit with sums of exponential time functions (see Eq. 1 and Fig. 4) by the Simplex fitting algorithm of pCLAMP. Rates of recovery from inactivation (e.g. Fig. 7C) were evaluated by fitting kinetic functions to test current peak amplitudes by least-squares regression (Table Curve 2D, Jandel Scientific, San Rafael, Calif., USA).

Series resistances typically measured less than 15 MΩ (range of values measured at beginning of current measurements from individual cells: 7–14 MΩ during perforated-patch recordings; 3.5–9 MΩ in ruptured-patch recordings). During measurement of decay kinetics, amplitude ratios of persistent to transient Na^+ current, and various current-voltage curves, series resistance compensation was employed at between 40 and 80%. Membrane potentials are reported without further correction for series resistance.

Results

We describe here the voltage-gated Na^+ current activated in single retinal ganglion cell somata by depolarizations for as long as 300 ms, from holding potentials between –100 and –15 mV, to test potentials between –75 and +80 mV. This current was measured in the presence of pharmacological agents that block voltage-gated Ca^{2+} currents, K^+ currents, and I_h (see Materials and methods). We have previously shown that the peak of current activated by brief (2–5 ms) depolarizations under these conditions reverses at membrane potentials near the Na^+ equilibrium potential, and that no appreciable inward current is carried by $Tris^+$ or by *N*-methyl-D-glucamine (NMG) [30]. As described below, Na^+ current activated by longer voltage steps appears to consist of at least two kinetic components. One reaches maximal amplitudes as large as 8 nA (4019±388 pA, 185±28 pA/pF, n=10), and decays along a rapid, exponential time course. The other is relatively small and most apparent as a non-decaying current (29±3 pA, 1.3±0.2 pA/pF, n=10) in whole-cell records at times later than 35 ms after the onset of depolarizations to test potentials between –45 and +40 mV (Figs. 1, 2). Currents exhibiting these kinetic profiles will be referred to below as "transient" and "persistent" Na^+ currents, respectively, without implying whether these currents arise from separate channel populations or not. Because these components differ in activation

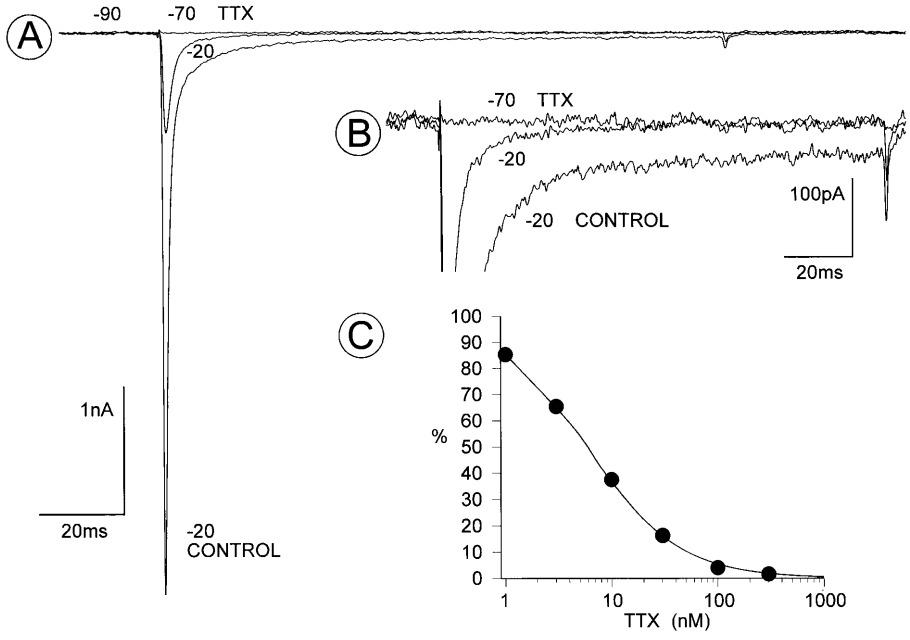

Fig 1A–C Tetrodotoxin (*TTX*). Na^+ current activated by depolarization from –90 mV to –20 mV before and after application of 20 nM TTX (traces marked control and TTX, respectively, in **A**, **B**). Note reduction of transient Na^+ current in **A**, and reduction of persistent Na^+ current at higher gain in **B**. Trace marked "–70" is current during voltage jump from –90 mV to –70 mV in the presence of TTX, included to show zero-current level. Calibration for all traces in **A** is positioned near the peak of transient current. **B** Currents truncated at –500 pA, and calibrated by mark at *lower right*. **C** Amplitude of Na^+ current activated in the presence of 1–300 nM TTX. Holding potential: –90 mV; test potential either –20 mV or –10 mV. *Filled circles* plot mean amplitude recorded from at least 3 cells at each TTX concentration, normalized to amplitude of current recorded before TTX application from each cell. The SEM at each TTX concentration is smaller than these *circles*. *Line* superimposed over measured values plots relative amplitude reductions calculated from the Hill equation, assuming a Hill number of 1.0 and a dissociation constant of 5.5 nM. Data included only if TTX block was reversible by wash, and only if the test depolarization elicited no outward current after a final application of 0.3–1 μM TTX (i.e., only if the leak conductance subtracted linearly at the test potential used). Two or three different TTX concentrations applied to each cell

threshold and resistance to steady-state inactivation, we initially assessed their TTX sensitivity, ion selectivity, and voltage sensitivity, using step-wise voltage jumps. We then measured the amplitude of Na^+ current activated and inactivated by spike-shaped changes in membrane potential.

Tetrodotoxin

TTX (0.3–1 μM) blocked both the decaying and non-decaying currents that activated regeneratively at test potentials between –65 mV and +20 mV (Figs. 1, 2). As in cardiac myocytes [44], moderate concentrations of TTX (10–20 nM) reduced the amplitude of persistent Na^+ current to immeasurably small levels, while leaving sizeable peak currents (Fig. 1B). However, the sensitivities of peak and persistent Na^+ current to TTX were not com-

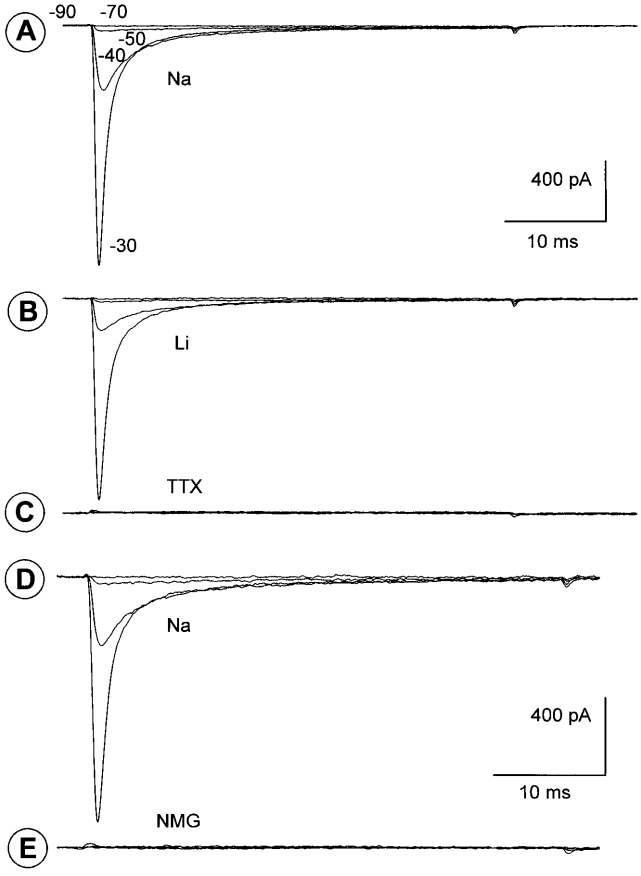

Fig. 2A–E Li^+ and *N*-methyl-D-glucamine (NMG^+). Current records in **A–C** activated by depolarizations of one ganglion cell in control Na^+-based bath solution, after replacement of bath Na^+ by Li^+, and after addition of 1 μM TTX to the Li^+ superfusate (*traces* labeled *Na*, *Li*, and *TTX*, respectively). The persistent current amplitudes in **A** and **B** are 20–40 pA. **D, E** Current records recorded from another ganglion cell in control saline and after replacement of bath Na^+ by NMG^+. No detectable outward current in **E** at the test potentials used. In all *panels*, holding potential is –90 mV; test potentials are –70, -50, -40, and –30 mV. *Calibration marks* for **A–C** and for **D**, **E** are positioned above **B** and **E**, respectively

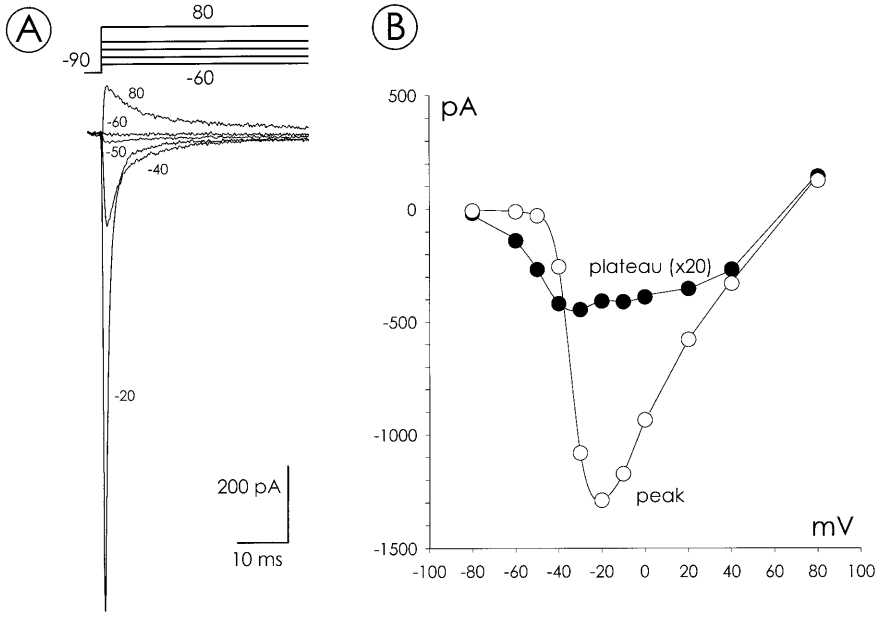

Fig. 3A, B Peak and plateau current-voltage plot. Na^+ currents in *lower part* of **A** activated by step depolarization from –90 mV to test potentials indicated next to each current trace (see *schematic* above *traces*). *Open* and *filled circles* in **B** plot amplitude of the current peak, and of the current at the end of each current trace (measured 38 ms after the beginning of each depolarizing step, and multiplied 20-fold for clarity), respectively, at each test potential. Current-voltage curves drawn through data by eye, cross *abscissa* near +67 mV

pared in detail, because the control amplitude of persistent Na^+ current was typically two or more orders of magnitude smaller than that of transient Na^+ current, and was therefore difficult to measure after reduction by TTX. Peak Na^+ current amplitudes in the presence of various TTX concentrations are plotted in Fig. 1C. Peak Na^+ current amplitude falls to 50% of control levels at a TTX concentration of 5.5 nM. The linear regression slope of a Hill plot constructed from these measurements is 1.0 (n_{Hill}, r^2=0.998).

In some cells, 1 µM TTX produced a slightly greater block of peak Na^+ current than did 300 nM TTX. However, we did not observe peak or persistent Na^+ current that resisted block by 1 µM TTX. This implies that the persistent inward current activated by depolarization under our recording conditions is not attributable to leak current subtraction errors, and that the Na^+ current we report here differs from TTX-resistant Na^+ currents found in various cells (e.g. [34]). Persistent inward Na^+ current was detectable in all cells, provided that activation of delayed outward currents did not result in current direction reversal during individual step depolarizations.

Selectivity

Li^+ could substitute for Na^+ as an inward current carrier. Li^+ currents (recorded after complete replacement of bath Na^+ by Li^+) were activated by depolarizations to test potentials between –60 and +20 mV; exhibited rapidly decaying, slowly decaying, and non-decaying components; and were suppressed by 300 nM TTX (Fig. 2). These currents were not markedly different in amplitude from Na^+ currents in the same cells (Figs. 2A,B), consistent with the relative permeabilities of Li^+ and Na^+ through Na^+ channels in other preparations [26]. Inward current was abolished by total, isosmotic replacement of Na^+ by NMG (Fig. 2E), consistent with the inability of methylated cations to carry detectable current through Na^+ channels in general [26].

The amplitude of the maximum (peak) current elicited at various test potentials and that of non-decaying current immediately before termination of each test depolarization (Fig. 3A) are plotted against test potential in Fig. 3B. Both of these current-voltage curves cross the abscissa between +65 and +70 mV, near the Na^+ equilibrium potential (+69 mV) estimated from the bath and pipette Na^+ concentrations used in this set of measurements (90 and 6 mM, respectively). These measurements (plus the effects of TTX, Li^+, and NMG described above) suggest that Na^+-permeable ion channels activated at all times during the test depolarizations used. Cahalan and Korn [10] have shown that an inward flux of Na^+ through delayed-rectifier K^+ channels can give rise to a persistent current during prolonged depolarizations. That type of Na^+ current is TTX resistant, carried poorly by Li^+, and blocked by patch-pipette solutions containing high concentrations of Cs^+. In all of these respects, that type of Na^+ current differs from the persistent Na^+ current we report here.

Decay kinetics

Having demonstrated that Na^+ current can be measured without substantial contamination by other voltage-gated currents, we next assessed its voltage sensitivity in terms of activation threshold, decay during sustained depolarizations, and steady-state inactivation. We first measured the decay of Na^+ currents activated by depolarizations to test potentials between –40 mV and +40 mV, from a holding potential of –90 mV. During step depolarizations lasting 45–300 ms, the decline of current from its peak value could be fit by the sum of a large, rapidly decaying

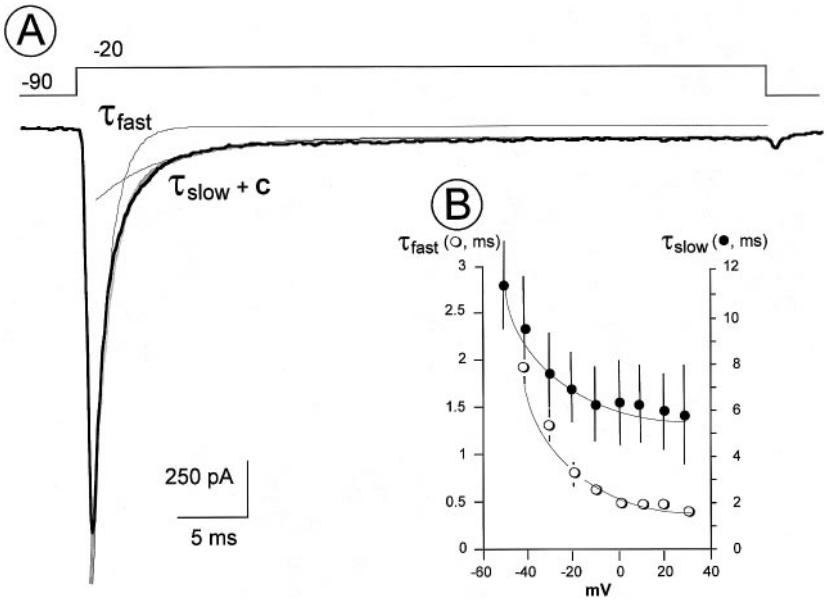

Fig. 4A, B Non-exponential current decay. Na^+ current (*bold trace*, *lower part* of **A**) activated by step depolarization from –90 mV to –20 mV (see *schematic* at *top* of *figure*). *Wide*, *light line* superimposed over current trace plots current calculated from Eq. 1 (see Results; beginning of fit can be seen near peak of inward current). *Thin line* marked "τ_{fast}" plots $A_{fast}\exp(-t/\tau_{fast})$, using τ_{fast} value determined by fitting algorithm (see Materials and methods); A_{fast} set by eye to maximize fit to rapidly decaying Na^+ current. Thin line marked "$\tau_{slow}+C$" plots values of $A_{slow}\exp(-t/\tau_{slow}) + C$. **B** τ_{fast} and τ_{slow} at test potential between –50 mV and +30 mV; means plotted by *open* and *filled circles*, respectively; *vertical bars* show ±1 SEM (n=5)

exponential, a small, gradually decaying component, and a non-decaying component. Figure 4 shows current activated by a 50-ms depolarization, and a fit by the following equation:

$$I_{Na} = A_{fast}\exp(-t/\tau_{fast}) + A_{slow}\exp(-t/\tau_{slow}) + C \quad (1)$$

where the peak amplitude and time constant of the fast and slow components are given by A_{fast} and τ_{fast}, and by A_{slow} and τ_{slow}, respectively, and C is the non-decaying (persistent) level. The faster exponential alone, and the sum of the slower exponential and constant terms are also overlaid over the current trace.

The more rapidly decaying exponential (τ_{fast}) fits the current trace for the first 2 ms after the current peak at –20 mV (Fig. 4A). This fit extends from the current peak to a point in time at which current has decayed to 1/3 of its peak amplitude. The current thereafter is larger than that plotted by the fast exponential. Most of this later current, from 7 ms after onset of the test depolarization to its end, is fit by the sum of the more slowly decaying and constant components (labeled $\tau_{slow} + C$). Moreover, the sum of these three components superimposes over the entire current trace. Sums of these three components yielded better fits than sums of two exponential functions or the sum of one exponentially decaying component plus a non-inactivating component.

The fast and slow time constants from the best fits of Eq. 1 to current traces from five cells are plotted in Fig. 4B. Both τ_{fast} and τ_{slow} decline substantially between –40 and 0 mV, and only slightly between 0 and +30 mV. A similar voltage sensitivity has been reported for τ_{fast} of cat and rat retinal ganglion cell Na^+ currents [5, 47]. Particularly at test potentials that activate the largest-amplitude Na^+ currents, the absolute values of τ_{fast} and τ_{slow} reported here are subject to distortion by uncompensated amounts of series resistance (see Materials and methods). However, the persistent Na^+ current we report here would not be attributable to series resistance or space clamp artifact (given the round shape of the somata we record from), nor would series resistance account for the tendency of the decay time constants to speed up with voltage (particularly when comparing equi-amplitude currents at different test potentials). In the remainder of this study, we compare the inactivation and activation of only the peak and persistent Na^+ currents.

Steady-state inactivation

Because currents like those fit in Fig. 4 by the constant term in Eq. 1 did not vanish during depolarizations as long as 300 ms, we used a double-pulse depolarization protocol to measure the amplitude of Na^+ current that resisted steady-state inactivation. Relatively long conditioning and test depolarizations (50–300 ms) were used, to facilitate collection of test currents after the rapidly decaying current faded, and to examine kinetics of the test current. The effect of conditioning depolarizations to membrane potentials between –95 and –15 mV are illustrated in Fig. 5. After the prepulse step to –65 mV, the test jump to –35 mV activated a rapidly decaying current that is roughly 50% smaller in amplitude than that activated from the holding potential (–95 mV; Fig. 5A). After the prepulse step to –15 mV, the current recorded during the jump to –35 mV was striking in two respects. First, it exhibited no substantial decay (Fig. 5A). Secondly, this current was identical in amplitude to that persisting at –35 mV after the conditioning step to –35 mV (Fig. 5A). The effects of conditioning membrane potential on the peak and sustained level of current activated at –35 mV are plotted in Fig. 5C. The plot shows that as the membrane potential during the conditioning voltage step is made more positive, the peak amplitude of the test current (at –35 mV) declines. However, the test cur-

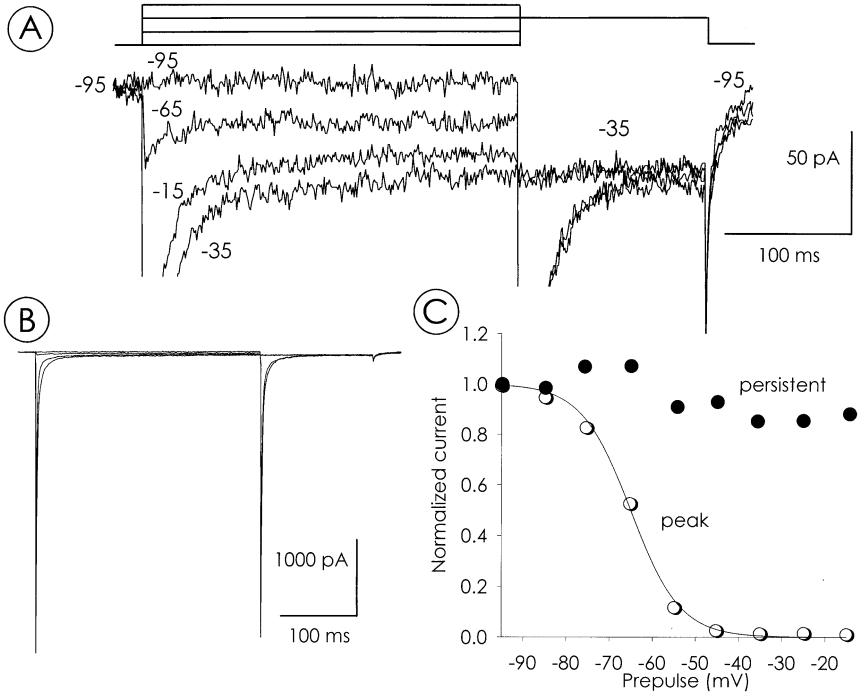

Fig. 5A–C Steady-state inactivation. Na^+ currents recorded at test potential of –35 mV, with and without 300-ms conditioning depolarizations to –65, -35, and –15 mV (see *schematic* at *top* of **A**). *Traces* in *lower part* of **A** are high-gain display of currents in **B**; inward currents exceeding –100 pA are truncated in **A**. **C** Current amplitude after termination of conditioning depolarization, at test potential of –35 mV, plotted against conditioning potential. Amplitudes measured at current peak and just prior to repolarization to holding potential (–95 mV), normalized to maximum value of the peak and non-decaying components respectively, and plotted by *open* and *filled circles* (labeled "*peak*" and "*persistent*"), respectively. Boltzmann distribution of values is plotted over the *open circles*; for pre-pulse potentials more positive than –35 mV, measured current amplitudes exceed calculated values. The conditioning membrane potential that reduced peak current amplitude at –35 mV to 50% of the control amplitude ($V_{1/2}$) was –59±2 mV (n=3) as in [5]. At a test potential of –10 mV, $V_{1/2}$ measured –47±4 mV (n=3) as in [33, 35, 47]

rent amplitude did not decline to zero at any of the conditioning voltages used. The Na^+ current that resisted inactivation (as in Fig. 5A) typically measured around 30 pA in maximum amplitude, i.e., 0.8±0.1% (n=10) of the maximum amplitude of the transient Na^+ current. Similarly small (or even smaller) fractions of the total TTX-sensitive Na^+ current are non-inactivating in a variety of cells [2, 12, 18, 22, 40, 42].

Activation

The most negative test potential that consistently activated measurable Na^+ current was –65 mV. Currents recorded at the end of long step depolarizations to –65 mV were similar in amplitude to those measured after hyperpolarizations to –65 mV from relatively positive conditioning potentials (Fig. 6A). The ratio of current amplitudes measured at a test potential of –65 mV, before and after conditioning depolarizations to –35 mV (as in Fig. 6A), was 1.0±0.1 (n=5). The currents at –65 mV (and also at –55 mV) are small enough that, at amplifier gains lowered to record peak Na^+ currents, activation may be noticed only at more positive membrane potentials (see open circles in Fig. 3B, and activation thresholds previously reported for retinal ganglion cell Na^+ currents [31]).

Because holding potentials between –90 and –60 mV did not markedly affect persistent Na^+ current amplitudes at test potentials between –70 and –35 mV (Figs. 5, 6), persistent Na^+ current showed no marked facilitation at these holding potentials. The activation range of persistent Na^+ current was measured under conditions that inactivated the transient Na^+ current. The Na^+ current at test potentials between –85 and –5 mV after 200-ms depolarizations to –35 mV are shown in Fig. 6B. Mean current amplitudes measured in several cells (n=5) are plotted against test potential in Fig. 6C. The most negative test potential that consistently activated measurable Na^+ current in this plot agrees with that measured with step depolarizations (Fig. 3).

Repeated depolarizations

Retinal ganglion cells can spike after dwelling at membrane potentials near spike threshold for several tens of milliseconds (see Fig. 8 in [4], and Fig. 3 in [47]), and after repolarizing to membrane potentials ranging between –50 mV and –25 mV between successive spikes (Fig. 7; see also [6, 53]). Because these membrane potentials are near (or more positive than) the midpoint of steady-state inactivation curves for transient voltage-gated Na^+ currents, Na^+ currents activated during spike

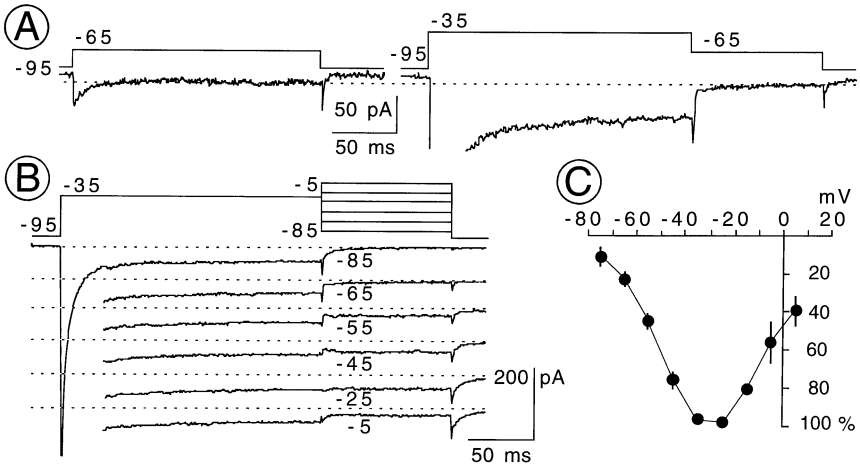

Fig. 6A–C Activation range. **A** Na^+ current at a test potential of –65 mV without (*left*) and with (*right*) 200-ms conditioning depolarization to –35 mV (see *schematic* above *traces*). *Dashed horizontal line* drawn across this pair of records to show similarity in current amplitude at –65 mV. **B** Na^+ current recorded at indicated test potentials after conditioning depolarization to –35 mV. *Traces* displaced vertically by arbitrary amounts; *dashed horizontal lines* position at zero-current level for each current trace. **C** *Dots* plot mean amplitude of currents recorded from 5 cells, at test potentials between –75 and +5 mV, after conditioning protocol shown above currents in **B**. *Vertical bars* plot ±1 SEM (if larger than *dot*). Current amplitudes normalized to maximum current amplitude recorded from each cell

trains are unlikely to be as large as those activated by step depolarizations from more negative holding potentials. This can be shown by calculations of Na^+ current amplitudes using Hodgkin-Huxley equations and spike-shaped depolarizing test potentials [15, 16], using the voltage sensitivities of activation and inactivation of the transient Na^+ current measured here (unpublished observations).

To more directly test this possibility, Na^+ currents were measured after spike- and ramp-shaped changes in membrane potential designed to mimic action potentials. As illustrated schematically in Fig. 7B, each of these potential changes consisted of a ramp-shaped "pre-potential" depolarization from membrane potentials *V*1 to *V*2, and a "spike" depolarization consisting of a fast depolarizing ramp from *V*2 to *V*3, and a repolarizing ramp from *V*3 to *V*4. *V*1, *V*2, *V*3, and *V*4 were set to the following values: *V*1, –70 mV, near published values of resting potential [6, 14, 30]; *V*2, –45 mV, because the rate of depolarization typically increased sharply at this membrane potential in current-clamp measurements of spikes (Fig. 7; see also [6, 17, 21]); *V*3, +15 mV, where spikes peaked during recorded trains (Fig. 7; see also [4, 21]); *V*4, –55 mV, because ganglion cells repolarize to membrane potentials as negative as –55 mV between successive spikes [6]. Rates of depolarization were set as follows: the pre-potential ramps were similar in duration to pre-potentials recorded under current-clamp mode (Fig. 7A). Spike rate of rise (40 *V*/s) was set to mimic rates of rise recorded from various retinal ganglion cell preparations (Fig. 7; see also [6, 14, 17, 36]).

The availability of Na^+ current for activation after spike-shaped depolarizations was measured in two ways. First, spike-shaped depolarizations were used as conditioning potentials, repeated once per 4–6 s. Each spike was followed by a ramp from *V*4 to *V*5 (from –55 mV to –45 mV, to mimic the shape of spikes like those in Fig. 7A) and then a single step-wise test depolarization (from *V*5 to 0 mV). Test depolarizations were presented as soon as 1 ms after the end of the conditioning depolarization, and the time between conditioning and test potentials was increased in 1- to 5-ms increments (e.g., the two voltage-change episodes superimposed in Fig. 7B). Varying this time from 1 to 60 ms enabled us to gauge the loss of Na^+ current available for activation after the first of several spikes firing in trains at frequencies between 16 and 250 Hz (calculated from the moments the test potential reached *V*2 and *V*5, and given that 3 ms elapsed between *V*2 and *V*4). Secondly, spike-shaped depolarizations were repeated at low frequencies to examine accumulation of inactivation during spike trains [13, 20, 32]. The Na^+ currents activated during all of the protocols used below were measured by digital subtraction of current recorded in the presence and absence of 1 µM TTX (without P/N leak subtraction).

Four properties of these Na^+ currents are illustrated by the current traces in Fig. 7C:

1. The TTX-sensitive current recorded throughout the course of these spike- and ramp-shaped depolarizations was inward, as expected because the test membrane potential was more negative than the Na^+ equilibrium potential at all times.
2. Na^+ current was inactivated in all cells (n=4) by the spike-shaped conditioning portion of the voltage change in Fig. 7B. At 1 ms after the end of these spikes, the test depolarization activated Na^+ currents that measured 951±377 pA in peak amplitude, 59±23 pA/pF in density, and 25±2% of the current amplitude activated by the conditioning spike. These test currents increased in amplitude as longer times separated the conditioning and test depolarizations. By 10 ms after the end of the conditioning spikes, the test Na^+ currents measured 1884±715

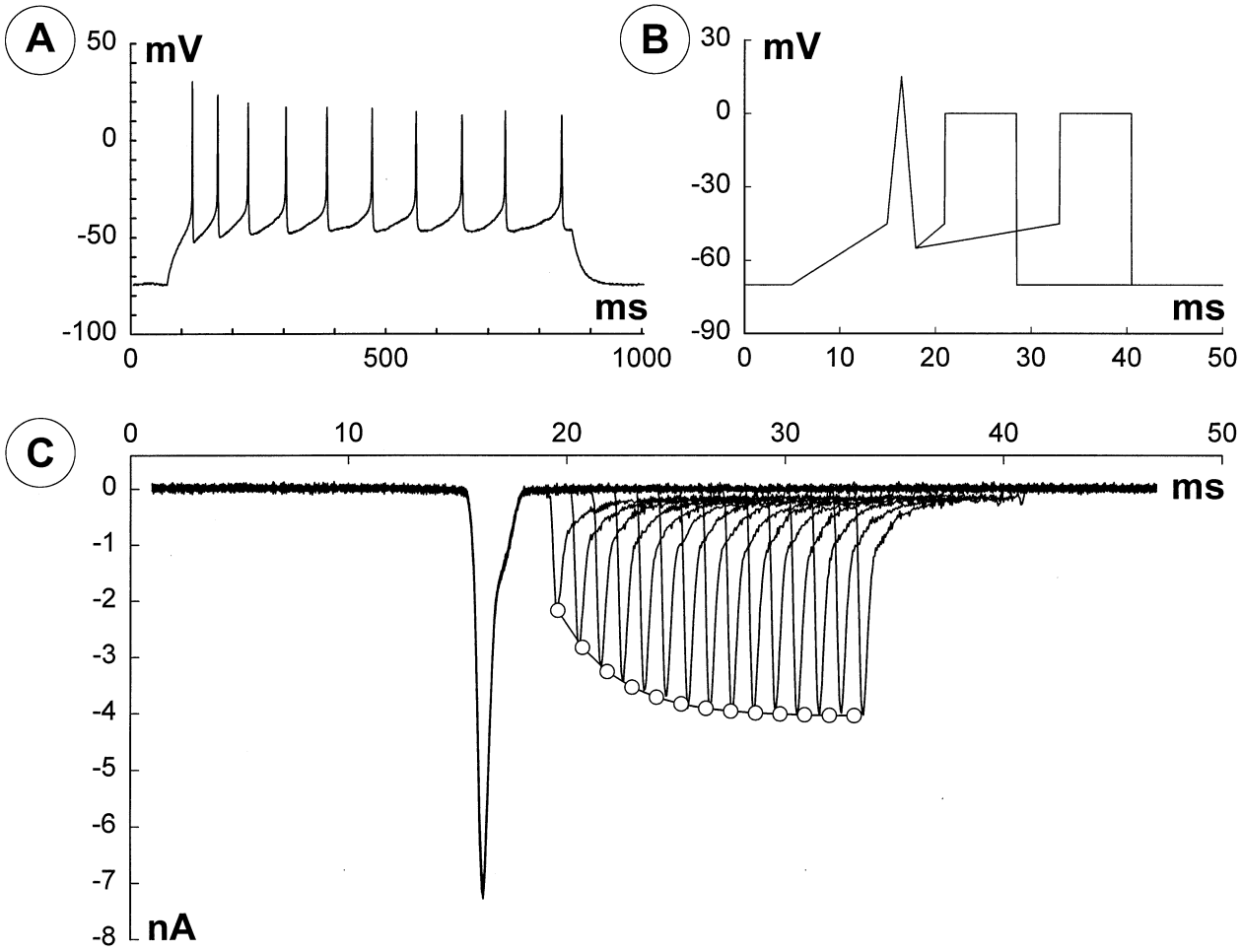

Fig. 7A–C Spikes and spike-shaped conditioning potentials. **A** Action potentials elicited by constant current injection through ruptured-patch recording pipette (99 pA). Bath solution consists of (in mM): 145 NaCl, 5 KCl, 2.5 $CaCl_2$, 10 D-glucose, 10 HEPES; pH 7.5. Pipette solution consists of (in mM): 145 KCl, 4 NaCl, 0.5 $CaCl_2$, 2 $MgCl_2$, 10 BAPTA, 10 HEPES; pH 7.5. **B** Two of the 15 command potential episodes used in **C** to measure Na^+ current recovery from inactivation by single action potentials. Each episode consists of a conditioning spike followed by a step-wise test depolarization (see text). Test currents measured as a function of time following spike. **C** Recovery of Na^+ current from inactivation by conditioning spike. Superimposed records of current activated in a single cell by 15 pairs of a spike and a 7.5-ms test depolarization. Spikes and test pulses are separated by between 1 and 15 ms in 1-ms increments (see text and **B**). Each *trace* is the difference between currents recorded before and after application of 1 μM TTX. *Circles* plot peak amplitudes calculated by Eq. 2, showing that Na^+ current recovers partially from inactivation along a quick, exponential time course (τ=2.6 ms). Currents activated by spikes show no change in amplitude or kinetics, indicating full recovery from rapid inactivation within time elapsed between successive conditioning pulses (4 s). Different cell than in **A**; Cs^+-based, perforated-patch pipette solution (see Materials and methods)

pA in peak amplitude, 118±21 pA/pF in density, and 51±3% of the current activated by the conditioning spike. Between 1 and 60 ms after the end of the conditioning spikes, these increases in test current followed an exponential time course. This phase of recovery from inactivation is illustrated by the 15 current records superimposed in Fig. 7C. The open circles plot values calculated from the equation:

$$I_{Na} = A + B[1 - \exp(-t/\tau)] \quad (2)$$

where A and B are constants, and t is the time elapsed after the end of the conditioning depolarization. This fit yields a time constant (τ) of 2.6 ms (r^2=0.993). Similar results were obtained in all cells tested (τ=3.0±0.5 ms; n=4), even though these cells ranged in membrane capacitance from 9 to 22 pF.

The initial recovery of Na^+ current from inactivation was also quick, exponential, and partial when the conditioning spike and test depolarization in Fig. 7B were replaced by 10-ms steps to –5 mV (and the first test currents were collected 1.5–2 ms after the end of the conditioning pulses). Similar time constants were obtained by fitting Eq. 2 to current amplitudes when (1) the membrane potential after termination of the conditioning depolarization, and until the beginning of the test depolarization, was fixed at –70 mV (τ=5.5±0.4 ms; n=9); (2) when this membrane potential and the holding potential were fixed at –100 mV (τ=4.7±0.3 ms; n=4); or (3) when the conditioning depolarizations were repeated once per 12 s (τ=4.9±0.3 ms; n=3). At 50 ms after the end of these 10-ms conditioning pulses, in cells held at –70 mV, test currents recovered to 82±3% (range: 64–90%) of the amplitude activated by the conditioning depolarization

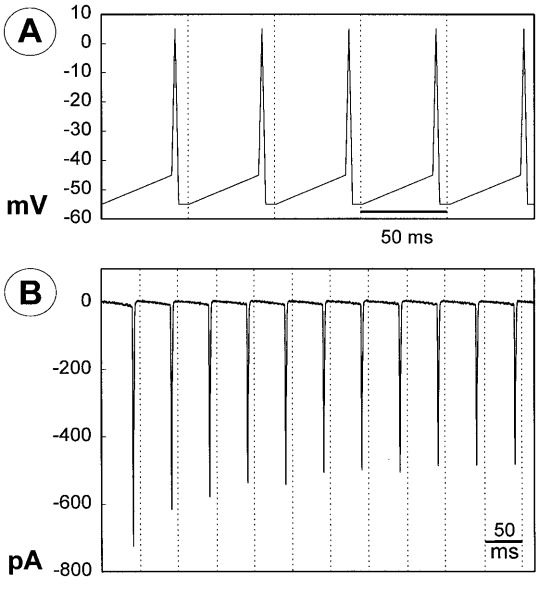

Fig. 8A, B Multiple spikes. **A** Five of the 11 identical spike-shaped depolarizations that activated the Na^+ currents in **B** (displayed in the order collected). In both **A** and **B**, each *panel* is 50 ms in duration, and a 60-ms interval separates the end of each *panel* from the beginning of the next *panel* (signified by each *dotted line*). Current traces are the difference between currents recorded before and after application of 300 nM TTX. Holding potential: –55 mV

(205±26 pA/pF). None of the above data were fit better by kinetic equations that incorporated a second exponential term.

3. As the amplitude of the peak Na^+ current increased after the termination of conditioning depolarizations, the amplitude of the persistent Na^+ current remained constant. In the traces of current activated by the test depolarizations in Fig. 7C, for example, portions of inactivation-resistant test current overlap neatly at an amplitude of roughly –125 pA (between roughly 23 ms and 41 ms in the superimposed records).
4. When repeated once per 4–12 s, depolarizations by the conditioning spikes and pulses activated Na^+ currents of constant amplitude (Fig. 7C). These currents thus appeared to recover completely from inactivation induced by brief conditioning depolarizations, within the shortest times that these conditioning depolarizations were repeated. We did not attempt to fit kinetic functions to the entire time course of this recovery, because we could not resolve contributions of slow inactivation at the holding potentials we used (see [28]).

Because Na^+ current appeared to recover completely from the inactivation induced by brief depolarizations within 4 s, but not within 50 ms, inactivation is expected to accumulate during conditioning depolarizations repeated at frequencies faster than those used in Fig. 7C. This was checked by depolarizing cells (n=5) with the spike waveform shown in Fig. 8A, with the holding potential set to –55 mV to mimic *V*4 in Fig. 7B. As illustrated in Fig. 8B, the currents activated by repetition of these spikes at 9 Hz declined in peak amplitude over a period of 200–300 ms. By the third spike after these 9-Hz "spike trains" commenced, the Na^+ current amplitudes measured 82±2% of those activated by the first spikes. Kinetic equations were not fit to these changes in current amplitude, because the intervals between test depolarizations were long. However, the decline in Na^+ current amplitude in Fig. 8B is roughly similar to the decline in spike amplitude in Fig. 7A.

Discussion

Our results demonstrate that voltage-gated Na^+ current is partially inactivated by both step-wise and spike-shaped depolarizations. Two conclusions are supported by our results. One is that the inactivation-resistant component of Na^+ current is not a "window" current in the cells we recorded from, because large depolarizations failed to fully inactivate it. This component of Na^+ current in retinal ganglion cells has not previously been described, and it would not have been predicted by previously reported activation and steady-state inactivation curves (see below). Secondly, at the interspike voltages we examined (*V*4 and *V*5 in Fig. 7), neither steady-state inactivation nor the initial phase of recovery from inactivation by brief depolarizations should preclude spike firing at frequencies as fast as several tens of Hz.

Non-exponential decay

Ensembles of Na^+ channels are expected to pass current persistently at membrane potentials where their activation and steady-state inactivation curves overlap. At more positive membrane potentials, homogeneous Na^+ channel populations that activate rapidly and have a single mean open-channel lifetime are expected to generate exponentially decaying ensemble Na^+ currents [1]. The whole-cell Na^+ current we recorded did not decay exponentially, and included a non-inactivating component at all membrane potentials more positive than activation threshold. This persistent Na^+ current does not seem due to space clamp inhomogeneity, or to excess subtraction of an inwardly rectifying leak current for three reasons: (1) the currents reported here were recorded from isolated somata, (2) the leak current subtracted linearly at the test membrane potentials used to study current activated by step-wise depolarizations, and (3) the current activated by protocols that included spike-shaped depolarizations were measured by subtraction of currents recorded in the presence and absence of TTX. The kinetics we have observed could have arisen from populations of rapidly inactivating Na^+ channels and physically distinct non-inactivating Na^+ channels [7, 23, 44, 55], *or* because a fraction of the inactivating Na^+ channel population failed to inactivate due to voltage-induced changes in gating kinetics [40].

Generality

The current density, decay time constant, and TTX sensitivity of the rapidly inactivating component of the total Na^+ current we report here do not differ markedly from those of previously described retinal ganglion cell whole-cell Na^+ currents [4, 5, 47]. However, the decay kinetics of Na^+ current activated by prolonged step depolarizations, and the extent of steady-state inactivation of the total Na^+ current we have measured differ from those reported previously for Na^+ current of amphibian, reptilian, and mammalian retinal ganglion cells. These previous studies report that Na^+ current decays exponentially during step depolarizations [5, 36, 47], and that activation and steady-state inactivation curves overlap by as much as 25 mV [33, 35, 38, 47]. These results predict that Na^+ current should fully decay at membrane potentials more positive than this 25-mV "window".

The presence of non-inactivating Na^+ current might explain two observations in studies of other retinal ganglion cell preparations. First, TTX has been found to hyperpolarize resting salamander and rat optic nerves [50, 52]. Secondly, although the Na^+ current of post-natal and adult retinal ganglion cell somata decays fully during step depolarizations [5, 35], one published inactivation (h_∞) curve suggests that some Na^+ current resists inactivation in embryonic cells (Fig. 11 in [47]). Thus, persistent Na^+ current may not be unique to fish retinal ganglion cells or to somata of retinal ganglion cells. The extent to which persistent Na^+ current accounts for the 20-mV spread in activation thresholds in various species [31], and whether similar fractions of Na^+ current resist inactivation in different structural compartments of retinal ganglion cells, remain to be assessed.

Recovery from inactivation

Our results show that Na^+ current recovery from inactivation is rapid, exponential, and partial over the first 50 ms following a brief conditioning depolarization. This pattern of recovery quantitatively and qualitatively resembles that of Na^+ current in other preparations [8, 20, 28]. In all of the cells we recorded from, this early phase of recovery was fit by a time constant (3 ms) that is remarkably similar to the most rapid of two fast time constants fitted to Na^+ current recovery after inactivation by 10-ms depolarizations of cat retinal ganglion cells [33]. In this respect, our results most closely resemble those obtained from a cell identified as having projected to cat lateral geniculate nucleus (Fig. 8A in [33]). None of our recovery measurements was fit better by a sum of two rapid exponentials, or solely by a significantly slower exponential, and thus differ from all other cat retinal ganglion cells described [33]. Our use of brief conditioning potentials (to mimic spikes) precludes comparison with the predominantly or exclusively slow recovery kinetics observed after long conditioning depolarizations [33, 54].

The current available for activation during spike trains will depend, in part, on the current density available in resting cells, the fraction of current that recovers from inactivation after single conditioning depolarizations, and steady-state inactivation at the voltages corresponding to *V*4 and *V*5 in Fig. 7B. At holding potentials set to typical values of resting potential (–70 mV), the Na^+ current densities we measured (205 pA/pF) exceed the amounts needed (in the absence of shunts) to depolarize cells at the maximum rates of rise we find during the first spike of trains recorded under current clamp (86±10 mV/ms, n=10 cells), and even at the fastest rates of rise recorded from retinal ganglion cells [6, 19]. Likewise, the Na^+ current in the cells we have studied should support several spikes at frequencies as fast as 100 Hz, because Na^+ currents return to 80% of control levels as rapidly as 10 ms after conditioning depolarizations, and because steady-state inactivation is roughly 50% between –45 and –55 mV.

Excitability

Our measurements of voltage sensitivity and current density suggest that transient and persistent Na^+ currents are geared to subserve at least two different functions. First, the amounts of Na^+ current available to be activated after single spikes are large enough to depolarize cells at rates observed in spikes recorded in various species (see above). The decline in Na^+ current amplitude during repeated spike-shaped depolarizations (Fig. 8) may contribute to the decline in spike amplitude seen in spike trains [13, 20, 32]. Secondly, the currents collected with step-wise voltage changes show that a fraction of the total Na^+ current activates at sub-threshold membrane potentials, and resists inactivation. Both of these properties are suitable for a variety of functions (especially triggering spike volleys, augmenting excitability, and amplifying small voltage changes; see [11, 23, 37, 46, 49]). For that matter, prior to the present study, I_h and T-type Ca^{2+} current were the only voltage-gated ion currents known to activate in retinal ganglion cells at membrane potentials between –100 mV and –50 mV [9, 31, 51]. Because I_h deactivates fully at membrane potentials more positive than –75 mV [51], and low-threshold Ca^{2+} current inactivates at membrane potentials more positive than –70 mV [9], Na^+ current is the only known voltage-activated ion current expected to flow persistently in retinal ganglion cells at membrane potentials between –65 mV and –45 mV.

Until the density and distribution of persistent Na^+ current in intact retinal ganglion cells is resolved, we refrain from speculation about the contribution of this component to spike output of retinal ganglion cells. However, we have recently found that the decay kinetics of Na^+ current are slowed by serotonin and by conditions that augment cytoplasmic levels of cyclic adenosine 3',5'-monophosphate [24]. The functional role of persistent Na^+ current in retinal ganglion cells may therefore

be synaptically or parasynaptically modulated, and conspicuous under conditions different from those used in the present study.

Acknowledgements This work was supported by National Institutes of Health grant EY 08120 from the National Eye Institute (Bethesda, Md., USA) to A.T. Ishida. We thank Professors Y. Hashimoto for the opportunity to pursue this study, and F.N. Quandt and P.A. Pappone for comments on our manuscript. We also thank A. Pignatelli for assistance during some of the experiments examining recovery from inactivation, and G.J. Partida for preparing the primary cell cultures used in these experiments.

References

1. Aldrich RW, Corey DP, Stevens CF (1983) A reinterpretation of mammalian sodium channel gating based on single channel recording. Nature 306:436–441
2. Alzheimer C, Schwindt PC, Crill WE (1993) Modal gating of Na^+ channels as a mechanism of persistent Na^+ current in pyramidal neurons from rat and cat sensorimotor cortex. J Neurosci 13:660–673
3. Attwell D, Cohen I, Eisner D, Ohba M, Ojeda C (1979) The steady state TTX-sensitive ("window") sodium current in cardiac Purkinje fibres. Pflügers Arch 379:137–142
4. Barres BA, Silverstein BE, Corey DP, Chun LLY (1988) Immunological, morphological, and electrophysiological variation among retinal ganglion cells purified by panning. Neuron 1:791–803
5. Barres BA, Chun LLY, Corey DP (1989) Glial and neuronal forms of the voltage-dependent sodium channel: characteristics and cell-type distribution. Neuron 2:1375–1386
6. Baylor DA, Fettiplace R (1979) Synaptic drive and impulse generation in ganglion cells of turtle retina. J Physiol (Lond) 288:107–127
7. Benoit E, Corbier A, Dubois JM (1985) Evidence for two transient sodium currents in the frog node of Ranvier. J Physiol (Lond) 361:339–360
8. Bezanilla F, Armstrong CM (1977) Inactivation of the sodium channel. I. Sodium current experiments. J Gen Physiol 70: 549–566
9. Bindokas VP, Ishida AT (1996) Conotoxin-sensitive and conotoxin-resistant calcium currents in fish retinal ganglion cells. J Neurobiol 29:429–444
10. Cahalan MD, Korn SJ (1994) Permeation of Na^+ through a delayed rectifier K^+ channel in chick dorsal root ganglion neurons. J Gen Physiol 104:747–771
11. Cannon SC, Brown RH Jr, Corey DP (1993) Theoretical reconstruction of myotonia and paralysis caused by incomplete inactivation of sodium channels. Biophys J 65:270–288
12. Chandler WK, Meves H (1970) Slow changes in membrane permeability and long-lasting action potentials in axons perfused with fluoride solutions. J Physiol (Lond) 211:707–728
13. Colbert CM, Magee JC, Hoffman DA, Johnston D (1997) Slow recovery from inactivation of Na^+ channels underlies the activity-dependent attenuation of dendritic action potentials in hippocampal CA1 pyramidal neurons. J Neurosci 17:6512–6521
14. Coleman PA, Miller RF (1989) Measurements of passive membrane parameters with whole-cell recording from neurons in the intact amphibian retina. J Neurophysiol 61:218–230
15. Connor JA, Stevens CF (1971) Prediction of repetitive firing behaviour from voltage clamp data on an isolated neurone soma. J Physiol (Lond) 213:31–53
16. Connor JA, Walter D, McKown R (1977) Neural repetitive firing. Biophys J 18:81–102
17. Diamond JS, Copenhagen DR (1993) The contribution of NMDA and non-NMDA receptors to the light-evoked input-output characteristics of retinal ganglion cells. Neuron 11: 725–738
18. Dubois JM, Bergman C (1975) Late sodium current in the node of Ranvier. Pflügers Arch 357:145–148
19. Eng DL, Gordon TR, Kocsis JD, Waxman SG (1990) Current-clamp analysis of a time-dependent rectification in rat optic nerve. J Physiol (Lond) 421:185–202
20. Fleidervish IA, Friedman A, Gutnick MJ (1996) Slow inactivation of Na^+ current and slow cumulative spike adaptation in mouse and guinea-pig neocortical neurones in slices. J Physiol (Lond) 493:83–97
21. Fohlmeister JF, Coleman PA, Miller RF (1990) Modeling the repetitive firing of retinal ganglion cells. Brain Res 510:343–345
22. French CR, Sah P, Buckett KJ, Gage PW (1990) A voltage-dependent persistent sodium current in mammalian hippocampal neurons. J Gen Physiol 95:1139–1157
23. Gilly WF, Armstrong CM (1984) Threshold channels – a novel type of sodium channel in squid giant axon. Nature 309: 448–450
24. Hidaka S, Ishida AT (1995) Modulation of voltage-gated Na^+ currents in retinal ganglion cells by serotonin receptor activation. Soc Neurosci Abstr 21:1035
25. Hidaka S, Ishida AT (1996) Non-inactivating, tetrodotoxin-sensitive sodium current in goldfish retinal ganglion cells. Invest Ophthalmol Vis Sci 37:1154S
26. Hille B (1992) Ionic channels of excitable membranes. Sinauer, Sunderland Mass., USA
27. Hodgkin AL, Huxley AF (1952) A quantitative description of membrane current and its application to conduction and excitation in nerve. J Physiol (Lond) 117:500–544
28. Howe JR, Ritchie JM (1992) Multiple kinetic components of sodium channel inactivation in rabbit Schwann cells. J Physiol (Lond) 455:529–566
29. Huguenard JR, Hamill OP, Prince DA (1989) Sodium channels in dendrites of rat cortical pyramidal neurons. Proc Natl Acad Sci USA 86: 2473–2477
30. Ishida AT (1991) Regenerative sodium and calcium currents in goldfish retinal ganglion cell somata. Vision Res 31:477–485
31. Ishida AT (1995) Ion channel components of retinal ganglion cells. Prog. Retinal Eye Res 15:261–280
32. Jung H-Y, Mickus T, Spruston N (1997) Prolonged sodium channel inactivation contributes to dendritic action potential attenuation in hippocampal pyramidal neurons. J Neurosci 17: 6639–6646
33. Kaneda M, Kaneko A (1991) Voltage-gated sodium currents in isolated retinal ganglion cells of the cat: relation between the inactivation kinetics and the cell type. Neurosci Res 11:261–275
34. Kostyuk PG, Veselovsky NS, Tsyndrenko AY (1981) Ionic currents in the somatic membrane of rat dorsal root ganglion neurons. Neuroscience 6:2423–2430
35. Lasater EM, Witkovsky P (1989) Membrane currents of spiking cells isolated from turtle retina. J Comp Physiol A 167:11–21
36. Lipton SA, Tauck DL (1987) Voltage-dependent conductances of solitary ganglion cells dissociated from the rat retina. J Physiol (Lond) 385:361–391
37. Llinás R, Sugimori M (1980) Electrophysiological properties of in vitro Purkinje cell somata in mammalian cerebellar slices. J Physiol (Lond) 305:171–195
38. Lukasiewicz PD, Werblin FS (1988) A slowly inactivating potassium current truncates spike activity in ganglion cells of the tiger salamander retina. J Neurosci 8:4470–4481
39. Magee JC, Johnston D (1995) Characterization of single voltage-gated Na^+ and Ca^{2+} channels in apical dendrites of rat CA1 pyramidal neurons. J Physiol (Lond) 481:67–90
40. Patlak JB, Ortiz M (1985) Slow currents through single sodium channels of the adult rat heart. J Gen Physiol 86:89–104
41. Patlak JB, Ortiz M (1986) Two modes of gating during late Na^+ channel currents in frog sartorius muscle. J Gen Physiol 87: 305–326
42. Quandt FN (1987) Burst kinetics of sodium channels which lack fast inactivation in mouse neuroblastoma cells. J Physiol (Lond) 392:563–585
43. Rodieck RW (1973) The vertebrate retina. Freeman, San Francisco

44. Saint DA, Ju Y-K, Gage PW (1992) A persistent sodium current in rat ventricular myocytes. J Physiol (Lond) 453:219–231
45. Sakmann B, Neher E (1995) Single-channel recording, 2nd edn. Plenum Press, N.Y.
46. Schwindt PC, Crill WE (1995) Amplification of synaptic current by persistent sodium conductance in apical dendrite of neocortical neurons. J Neurophysiol 74:2220–2224
47. Skaliora I, Scobey RP, Chalupa LM (1993) Prenatal development of excitability in cat retinal ganglion cells: action potentials and sodium currents. J Neurosci 13:313–323
48. Strafstrom CE, Schwindt PC, Crill WE (1982) Negative slope conductance due to a persistent subthreshold sodium current in cat neocortical neurons in vitro. Brain Res 236:221–226
49. Stuart G, Sakmann B (1995) Amplification of EPSPs by axosomatic sodium channels in neocortical pyramidal neurons. Neuron 15:1065–1076
50. Stys PK, Sontheimer H, Ransom BR, Waxman SG (1993) Noninactivating, tetrodotoxin-sensitive Na^+ conductance in rat optic nerve axons. Proc Natl Acad Sci USA 90:6976–6980
51. Tabata T, Ishida AT (1996) Transient and sustained depolarization of retinal ganglion cells by I_h. J Neurophysiol 75: 1932–1943
52. Tang CM, Strichartz GR, Orkand RK (1979) Sodium channels in axons and glial cells of the optic nerve of *Necturus maculosa*. J Gen Physiol 74:629–64
53. Taschenberger H, Grantyn R (1995) Several types of Ca^{2+} channels mediate glutamatergic synaptic responses to activation of single Thy-1-immunolabeled rat retinal ganglion neurons. J Neurosci 15:2240–2254
54. Wang G-Y, Ratto G-M, Bisti S, Chalupa LM (1997) Functional development of intrinsic properties in ganglion cells of the mammalian retina. J Neurophysiol 78:2895–2903
55. Westenbroek RE, Merrick DK, Catterall WA (1989) Differential subcellular localization of the R_I and R_{II} Na^+ channel subtypes in central neurons. Neuron 3:695–704
56. White JA, Sekar NS, Kay AR (1995) Errors in persistent inward currents generated by space-clamp errors: a modeling study. J Neurophysiol 73:2369–2377